UCRL-TR-209954

High-Energy Neutron Imaging Development at LLNL

J. M. Hall (PI), B. Rusnak (PE) and S. Shen

Lawrence Livermore National Laboratory

24 February 2005

FY04 Annual Report submitted for ESC project LL-24

Disclaimer

Auspices Statement

This work was performed under the auspices of the U. S. Department of Energy (DOE) by the University of California, Lawrence Livermore National Laboratory (LLNL) under Contract No. W-7405-Eng-48.

High-Energy Neutron Imaging Development at LLNL

James Hall (PI), Brian Rusnak (PE) and Stewart Shen

Lawrence Livermore National Laboratory, P.O. Box 808, M/S L-050, Livermore, CA 94551-9900

Abstract We are proceeding with the development of a high-energy (10 MeV) neutron imaging system for use as an inspection tool in nuclear stockpile stewardship applications. Our goal is to develop and deploy an imaging system capable of detecting cubic-mm-scale voids, cracks or other significant structural defects in heavily-shielded low-Z materials within nuclear device components. The final production-line system will be relatively compact (suitable for use in existing facilities within the DOE complex) and capable of acquiring both radiographic and tomographic (CT) images. In this report, we will review our recent programmatic accomplishments, focusing primarily on progress made in FY04. The design status of the high-intensity, accelerator-driven neutron source and large-format imaging detector associated with the system will be discussed and results from a recent high-energy neutron imaging experiment conducted at the Ohio University Accelerator Laboratory (OUAL) will also be presented.

INTRODUCTION

We are proceeding with the development of a high-energy (10 MeV) neutron imaging system for use as an inspection tool in nuclear stockpile stewardship applications associated with the DOE Enhanced Surveillance Campaign (ESC). Our goal is to develop and deploy an imaging system capable of detecting cubic-mm-scale voids, cracks or other significant structural defects in heavily-shielded low-Z materials within nuclear device components. Potential applications for this new diagnostic include: (1) collection of "baseline" data characterizing the "as-designed" vs. "as-built" configurations of stockpiled units (relevant to ESC Campaigns 4 & 6), (2) routine surveillance of stockpiled units (relevant to Directed Stockpile Work (DSW)), (3) inspection and/or re-certification of nuclear device components (relevant to Stockpile Lifetime Extension Programs (SLEPs)), (4) non-destructive damage assessment (relevant to Stockpile-to-Target Sequence (STS) engineering tests) and (5) identification of specific devices for potential stockpile reductions if mandated. Note that our intent is to develop an inspection system that will *complement* - not replace - existing ESC x-ray diagnostic tools.

The final production-line imaging system will be relatively compact (suitable for use in existing facilities within the DOE complex) and capable of acquiring both radiographic and tomographic (CT) images. It will consist of an intense, accelerator-driven D(d,n)^{3}He neutron source ($E_n \approx 10$ MeV @ 0°) with an effective yield of $\approx 10^{11}$ n/sec/sr along the beam axis and an effective focal spot size of ≈ 1.50 mm (FWHM), a multi-axis staging system to support and manipulate objects under inspection and a neutron imaging detector (*cf.* Figure 1). The detector itself will consist of a transparent plastic scintillator (*e.g.* BC-408) viewed indirectly by one or more high-resolution CCD or CMOS cameras. The ultimate spatial resolution of the imaging system will depend on the details of the final design but should be ≈ 1.00 mm (FWHM) at the object position.

The conceptual design of the imaging system and results from several previous imaging experiments have already been published in the open literature [1 - 6] and previous ESC reports. In this report, we will review our recent programmatic accomplishments, focusing primarily on progress made in FY04. The design status of the neutron source and imaging detector associated with the system will be discussed and results from a recent high-energy neutron imaging experiment conducted at the Ohio University Accelerator Laboratory (OUAL) in Athens, OH, will also be presented.

SOURCE DEVELOPMENT

The development of an intense, high-energy neutron source suitable for use in a full-scale, production-line imaging system is critical to the success of this project. As noted above, we propose to use an accelerator-driven D(d,n)^{3}He neutron source operating at ≈ 10 MeV. In order to meet our performance requirements, the source will need to have an effective yield of $\approx 10^{11}$ n/sec/sr along the beam axis and an effective focal spot size of ≈ 1.50 mm (FWHM). While this is certainly achievable using existing (*i.e.* commercial and low-risk) technologies, it does pose some challenging technical problems, particularly in the design of the D_2 gas target endstation and residual beam stop.

Accelerator Design

The accelerator system that we propose to use in our full-scale neutron source will be based on mature, commercially-available technology. It will consist of a D^+ ion source and a pair of compact radio-frequency quadrupoles (RFQs) coupled to a short drift-tube linac (DTL) (*cf.* Figure 2). The system must accelerate D^+

ions to an energy of ≈ 7 MeV and be capable of delivering an average ion current of ≈ 320 μA to a D_2 gas cell located in the target endstation in order to generate a neutron yield sufficient for our imaging applications. The beam pulse frequency needs to be ≈ 100 Hz in order to facilitate coupling with the endstation and the duty factor should be ≈ 1.95% (this implies a peak current of ≈ 15 - 17 mA and a pulse width of ≈ 195 μsec). The overall emittance ($\varepsilon_{x,y}$) of the beam must also be ≤ 3.3 mm-mrad in order to achieve the small focal spot size required at the endstation.

The full-up design of the accelerator system was completed during Q4 of FY02 by the proposed vendor, AccSys Technologies, Inc. of Pleasanton, CA, under a sole-source contract from LLNL. It was subsequently reviewed and accepted by the project PE during Q1 of FY03. The projected cost of the system at that time was ≈ $2.5M and the estimated lead time for fabrication and delivery was ≈ 12 months [7].

HEBT System

The initial (conceptual) design of the high-energy beam transport (HEBT) system needed to transport and focus D^+ ions from the accelerator into the target endstation was developed using the charged particle transport code TRACE3D during Q1 of FY03 (*cf.* Figure 3); however, based on guidance from ESC management at LLNL, we have elected to focus our effort and available funding since that time on the development of other system components involving relatively higher technical risk and/or longer lead times. Finalizing the design of the HEBT system (*i.e.* identifying specific, commercially-available focusing elements compatible with our beam transport requirements and then integrating them into the overall system design) is not expected to be a particularly challenging problem. Depending on project funding and ESC priorities, we hope to address this issue sometime in FY06.

Endstation Design

The simultaneous requirements for a large D^+ ion current and relatively small focal spot size imposed by our proposed imaging application effectively preclude the use of a conventional (*i.e.* "windowed") D_2 gas cell in the target endstation since there currently exist no window materials capable of handling the relatively large areal power densities involved (≈ 125 kW/cm^2 (average) in our case). We have therefore focused our effort on the development of "windowless" D_2 gas cell designs which could potentially be incorporated into the endstation and coupled to a pulsed accelerator system for use as an intense neutron source.

The most promising way to handle the large areal power densities anticipated appears to be with the use of a "rotating-aperture" (RA) gas cell. In this approach, narrow (≈ 4 - 5 mm diameter) entrance and exit apertures on the high-pressure (≈ 3 atma) gas cell (and any adjacent differential pumping stages) are "open" only when they coincide with matching apertures in a series of rotating disks synchronized to the pulse frequency of the accelerator beam. This effectively isolates the high-pressure gas in the cell from the accelerator vacuum system. Pioneering research conducted at MIT [8 - 11] has shown that even a rudimentary RA system can create a very effective "plug" between a pressurized gas cell and a differential pumping system and work done at the DeBeers Diamond Research Laboratory in South Africa [12] has since proven the effectiveness of these systems in production-line applications.

Our initial RA target endstation design was based on a contained, "turbulent-volume" approach similar to that used in the early work at MIT (*cf.* Figure 4). The rotating apertures were immersed in the high-pressure D_2 target gas in this design in order to facilitate sealing and minimize pressure-induced pulsing of the rotors. It was thought at the time that placing the rotors inside the cell would also induce turbulent mixing in the gas and thereby improve convective cooling.

While this approach initially seemed to be a viable way to contain the high-pressure D_2 gas, there were still concerns that even the combination of turbulent mixing and convective cooling would be insufficient to prevent density rarefactions in the target gas due to beam heating ("burn through"). Subsequent fluid hydrodynamics calculations done with LLNL's ALE3D code indicated that this was, in fact, the case. For peak beam currents in the 5 - 20 mA range, significant heating of the target gas was found to occur within 10's of μsec, causing a rapid drop in density along the beam channel (*cf.* Figure 5) and an attendant decrease in the neutron yield that one might normally expect for a given incident beam current and gas cell pressure (*cf.* Figure 6).

Following a formal Engineering Design Review of this system conducted at LLNL during Q3 of FY02, we revised the design of the target endstation to incorporate a means to rapidly refresh the beam channel with cool D_2 gas at the required density in an effort to mitigate beam heating effects. Our new, single-stage design now features a cross-flow D_2 venturi capped at either end by baffled, rotating apertures (*cf.* Figure 7). If the venturi is designed to generate a high enough flow rate (≈ 200 - 250 m/s), the D_2 gas in the beam channel (≈ 1.50 mm FWHM) can be effectively refreshed ≈ 25 - 30 times during the course of a single beam pulse (≈ 195 μsec). Additional ALE3D calculations done during FY04 have confirmed that it should be possible to maintain a D_2 gas density in the beam channel equivalent to an average pressure of ≈ 3 atma using reasonably-sized, commercially-available vacuum pumps and standard gas handling systems (*cf.* Figure 8). This, in turn, should

allow us to maintain a neutron yield from the source close to the required level (*cf.* Figure 9).

Our revised endstation design actually offers several major advantages over the initial design. The first comes from the fact that we are now able to use a one-piece, rigid sub-frame to align and hold all of the various precision parts that need to rotate at ≈ 4000 RPM. This eliminates the need to procure or fabricate special vacuum enclosures that can also be precision aligned. Second, by using a vacuum-rated motor located *inside* of the high-pressure stage of the endstation, we eliminate the need for Ferrofluidic vacuum seals, which can become complicated to use at higher rotational speeds since they may need to be water cooled (there were also concerns about the ultimate reliability of these seals in high-radiation environments). Finally, the proposed use of internal baffles (essentially "mufflers") in the rotors on the high-pressure gas cell should help to damp out sonic pressure waves that may emitted along the beam axis as the apertures open and close during operation. This should help to further reduce the base pressure in the endstation, hopefully to a level low enough to allow it to be coupled directly to the HEBT system without the need for additional vacuum pumps.

The basic design of the new cross-flow D_2 venturi endstation was actually completed during Q1 of FY03; however, unanticipated ESC budget shortfalls during FY03 prevented us from finalizing the design that year. With restored funding, the final design package was quickly completed during Q1 of FY04 and two full-scale prototypes of the endstation suitable for use in testing were subsequently fabricated by a precision machine shop, the CHAMP Company of Campbell, CA, under a sole-source contract from LLNL. The first of these units was delivered at the end of Q3 (*cf.* Figure 10) and installed in a custom-designed vacuum enclosure equipped with a variety of sensors for diagnostic purposes (*cf.* Figure 11).

One of the primary goals in designing and fabricating these initial test units was to verify that we could, in fact, achieve a gap spacing of ≈ 0.001" between a high-speed rotor and stator *(i.e.* the venturi in our case). The width of the gap will be a critical factor in mitigating leak rates from the high-pressure gas cell and maintaining base pressure as low as possible in the endstation; however, achieving such a tight tolerance requires not only high-precision in the machining of components but also very careful attention to detail in their assembly. In order to facilitate making these gap measurements, the venturi that would be normally used in an actual production unit has, for the time being, been replaced by a rectangular cross-flow tube with a single aperture and a straight throat that can be used in tests with static gas (*cf.* Figure 12). The opposing surfaces of the rotors and cross-flow tube were all hard anodized with alumina, allowing them to be lapped and then precision ground for smoothness and flatness (it was also thought that anodizing these surfaces would help to prevent galling and/or seizing in case the surfaces inadvertently came in contact while the rotors were spinning at high RPM). The cross-flow tube also features a series of grooves machined on the bottom into which heaters can be installed to control the temperature of the block, thereby providing us with a "fine-adjust" knob on gap spacing via thermal expansion if needed.

We began to conduct performance tests on the first of these units in Q4 of FY04, following a previously-devised test plan, and quickly verified that the rotating machinery part of the assembly worked as designed in vacuum. The drive motor temperature was stable as the system ran for a number of hours at up to 4000 RPM; however, problems arose when we began to pressurize the cross-flow tube with gas. Our initial measurements, taken using N_2 and He as surrogates for D_2 for safety reasons, were very encouraging. Testing continued until, after several minutes of running at gas pressures of up to ≈ 3 atma, the system suddenly seized up - going from 1000 RPM to zero in an instant.

Subsequent disassembly and forensic examination revealed that the failure was caused by a gradual build-up of powdered alumina between the rotor and stator, which slowly filled the narrow gap and increased drag. This eventually caused the system to seize up entirely, resulting in appreciable scoring on the surfaces of both the rotor and cross-flow tube (*cf.* Figure 13). The source of the powder was discovered to be residual deposits of hardened alumina "mud" that had accumulated in the baffles of the rotors during the original surface grinding process and which were apparently unimpressed by our feeble attempts to remove them using standard cleaning techniques (including ultrasonic baths in water and alcohol) prior to assembly; however, high-pressure shock waves passing through the apertures of the rotor during operation apparently *did* manage to gradually dislodged the deposits and pulverize them into a fine dust, which was then generously redistributed throughout the entire vacuum enclosure (*cf.* Figure 14).

In spite of the damage done to the surfaces of the rotor and cross-flow tube on this unit, additional data was taken with it in an effort to debug the system and improve our diagnostic techniques. The initial data that we got, even with damaged surfaces, was very encouraging (*cf.* Figure 15) and indicates that we should be able to maintain a base pressure of < 10 - 20 torr in the high pressure pumping stage of the endstation using a few relatively inexpensive dry scroll pumps. Additional measurements, done on a test unit with pristine surfaces in close tolerance (*i.e.* ≈ 0.001"), will need to be done to further refine this result (note that our eventual goal is to reduce the base pressure in the endstation to ≤ 5 torr with ≈ 3 atma in the venturi of the gas cell). In the

mean time, having been unable to reliably remove the residual deposits of alumina "mud" in the baffles of our current test units, we have temporarily elected to replace the baffled rotors with solid rotor assemblies with simple through holes for apertures. Work is now proceeding on characterizing the performance of the endstation using these rotors. We expect to complete our current suite of tests involving the use of static gas in the prototype units by Q3 of FY05 and should be able to finalize the endstation design by the end of the FY. The high-pressure gas handling system needed to run performance tests with the cross-flow venturi in place will be designed in late FY05 and should be ready for use sometime in FY06.

The laboratory research activities described in this section were carried out under the auspices of an approved Integrated Work Sheet (LLNL IWS # 11618, *Prototype Rotating Aperture System*, RI: S. Shen) and in accordance with a related Engineering Safety Note and all applicable LLNL facility Operating Safety Procedures. Copies of these documents and/or additional information on personnel safety issues related to this work may be obtained directly from the authors of this report upon request.

Beam Stop

After the incident ion beam passes through the D_2 gas cell in the endstation, it needs to be dissipated in a way that not only has minimal impact on the intensity and spatial distribution of the primary (monoenergetic) neutrons generated in the gas cell, but also produces as few additional (broad-spectrum) neutrons as possible. The design of a beam stop suitable for use with the endstation is recognized as an important technical problem; however, while several reasonably low-risk approaches appear promising, this has yet to be addressed in sufficient detail to finalize a design. Based on guidance from ESC management at LLNL, we have again elected to focus our effort and available funding thus far on the development of other system components involving relatively higher technical risk and/or longer lead times. We hope to address this issue in FY06.

IMAGING DETECTOR

The development of a high-efficiency, large-format neutron detector suitable for use in a full-scale, production-line imaging system is also critical to the success of this project. While the prototype detector developed for use in our experiments at OUAL has worked quite well thus far, allowing us to validate the potential of neutron imaging by capturing radiographic and tomographic images of a variety of test objects, its format is only ≈ 30 cm X 30 cm. The full-scale detector that we envision will need to have a format ≈ 2 - 3 times this size in order to meet the requirements of potential ESC inspection scenarios. As noted above, the detector will consist of a plastic scintillator (*e.g.* BC-408) viewed indirectly by one or more high-resolution CCD cameras. The ultimate spatial resolution of the imaging system will depend on the details of the final design but should be no worse than ≈ 1.00 mm (FWHM) at the object position. While not as good as some x-ray imaging systems, this is considered to be adequate for most proposed ESC applications.

A preliminary design study related to the development of the full-scale imaging detector was completed during Q4 of FY04 by the proposed vendor, Optics1, Inc. of Westlake Village, CA, under a sole-source contract from LLNL. This study focused primarily on two different design options currently under consideration (*cf.* Figure 16) and involved identifying suitable sensors, designing fast optical lens systems and defining predicted resolutions and photon error budgets (*i.e.* signal-to-noise (S/N) ratios) for each case.

Design option 1 utilizes an array of four overlapping 2048 X 2048, 24 μm pixel, TE-cooled, CCD cameras to image an 85 cm X 85 cm field-of-view at the scintillator. This design is similar to that currently being built by Optics1 for use in ESC high-resolution x-ray imaging systems at Pantex and would allow us to image objects of interest at a geometrical magnification factor of ≈ 2:1 (which minimizes image noise caused by internal scattering within the object). Image registration would be done using a dedicated control computer with final processing and analysis being done off-line in a secure environment. The predicted S/N ratio for this design option is ≈ 1.3X that of our current prototype imaging detector at OUAL.

Design option 2 utilizes a single 4096 X 4096, 15 μm pixel, TE-cooled, CCD camera to image a 65 cm X 65 cm field-of-view at the scintillator. This design is larger in scale but conceptually similar to that currently being used in our imaging experiments at OUAL and should provide optical resolution comparable to that of option 1; however, its somewhat smaller field-of-view will require us to image at a geometrical magnification factor of ≈ 1.25:1 instead of 2:1. While this might result in a slight increase in image noise due to internal scattering within the object, it should also decrease the projected source spot size at the image plane, thereby allowing us to push the ultimate spatial resolution at the object position below 1.00 mm (FWHM). The predicted S/N ratio for this design is ≈ 82X that of our current prototype imaging detector at OUAL. Due to its inherent simplicity, lower cost and higher predicted performance, this option is our current favorite. We expect to issue a contract to a qualified vendor to fabricate a full-scale prototype of this detector during Q2 of FY05 and hope to be able to run acceptance tests on it at OUAL sometime before the end of the FY.

RECENT EXPERIMENTS

We conducted one neutron imaging experiment at OUAL during FY04. The experiment was funded by the DOE Pantex Plant via a Work-for-Others (WFO) contract awarded directly to the project PI (Hall) and involved tomographic imaging of an unclassified test object containing Insensitive High Explosives (IHE). The primary purpose of the experiment was to further assess the potential of using high-energy neutron imaging as a quality-control and/or surveillance diagnostic tool in the High Explosives NDE program at Pantex. The current technique used to detect defects such as density variations and void formations in HE components within weapons systems at Pantex is destructive (*i.e.* selected devices are disassembled and samples of the explosives are removed and measured to determine their actual weight and volume). Neutron imaging is one of several new NDE techniques being investigated by Pantex personnel to supplement (or possibly replace) this destructive inspection procedure.

The setup of the experiment was similar to that described in previous reports. A nearly monoenergetic, 10 MeV neutron beam was generated by focussing 6.85 MeV D^+ ions extracted from OUAL's tandem van de Graaff accelerator into a cylindrical D_2 gas cell, 1 cm in diameter and 8 cm long, attached to the end of a beam line. The gas cell was capped with a thin (≈ 5 μm) W entrance window and maintained at a static pressure of ≈ 45 psia (≈ 3 atma). The average D^+ ion current at the gas cell was ≈ 6.5 μA during each of the imaging runs. This corresponds to an estimated 10 MeV neutron yield of ≈ $4x10^9$ n/sec/sr along the beam axis (*i.e.* ≈ $1/25^{th}$ of the intensity of the source proposed for our full-scale system). The effective focal spot size of the beam was ≈ 3 mm (FWHM) at the entrance window to the gas cell (*i.e.* ≈ 2X that of the source proposed for our full-scale system). The test object was placed on a rotation stage ≈ 200 cm from the neutron source and ≈ 200 cm from the imaging detector, resulting in a geometric magnification factor of ≈ 2:1 at the image plane. The imaging detector consisted of a 30 cm X 30 cm X 4 cm thick BC-408 transparent plastic scintillator viewed indirectly by a single high-resolution (1024 X 1024; 24 μm pixel), LN_2-cooled, CCD camera equipped with a high-speed (f/1.0) commercial photographic lens.

The test object consisted of a stack of three PBX-9502 IHE samples uniformly pressed to different densities within a relatively narrow range (≈ 1.84, 1.87 and 1.90 g/cc) and bonded together to form a single 2.00" high annular cylinder with a 2.00" OD and 0.375" ID. The IHE stack was surrounded by a 0.125" thick high-Z (U6%Nb) clamshell and had a low-Z (Be) sleeve with a 0.125" wall thickness inserted along its centerline (*cf.* Figure 17). A 0.050" thick Silastic pad with an array of eight holes ranging in size from 1.00" down to 1/64" was also sandwiched in between the U6%Nb clamshell and the IHE (just visible in the photo in Figure 17). The final assembly was mounted on a low-mass aluminum stand securely attached to the rotation stage and imaged perpendicular to its principal axis.

Tomographic imaging of the test object was done using a new high-precision, computer-controlled rotation stage interfaced to our existing data acquisition system at OUAL. The new control system (driven using a simple LabView script) is fully automated, virtually immune to neutron source faults (*i.e.* temporary or even long-term loss of beam) and capable of taking interleaved CT data sets consisting of 4, 8, 16, 32, 64, 128, *etc.* views of a test object at equally spaced angular intervals over 360º. The full CT data set in this case consisted of a series of 128 20 minute exposures taken over 360˚ (Δ = 2.8125˚). The individual images were of reasonably good quality (*cf.* Figure 18) and revealed the basic structure of the test object.

The CT data set obtained during this experiment was subsequently processed using LLNL's Constrained Conjugate Gradient (CCG) cone-beam reconstruction algorithm, a portion of the development of which has been funded by this project. The CCG algorithm utilizes an iterative, constrained (*e.g.* $\mu X \geq 0$) least-squares fitting procedure which, while more CPU intensive than Conventional Back Projection (CBP) algorithms, significantly reduces the overall statistical noise level in CT reconstructions (*cf.* Figure 19).

Horizontal and vertical slices taken through CCG reconstructions of the IHE test object again revealed its basic structure, including even the bond joints between the three IHE segments (*cf.* Figure 20); however, neither the small density differences between the segments (≈ 0.03 g/cc) nor any of the holes in the 0.050" Silastic pad were discernable. The reasons for this failure are somewhat puzzling, particularly since we were easily able to discern (and even quantify) IHE density differences as small as 0.05 g/cc and holes in shielded Silastic padding ≥ 1/8" in diameter in radiographic imaging experiments done on another test object at OUAL during FY03, although it seems likely that relatively poor counting statistics and inadequate angular resolution (*i.e.* an insufficient number of CT views) were contributing factors. On the other hand, we *could* simply be at the limit of what of our prototype detector at OUAL can do in terms of this type of imaging.

We should note in passing that our original intent going into this experiment was to take a series of 256 30 minute images of the test object at equally spaced angular intervals over 360˚ (Δ = 1.40625˚). This would have provided us with better statistics and improved angular resolution in the CT reconstructions; however, the OUAL accelerator system was *very* unstable this time out (as the song goes, "Some days are diamonds,

some days are rust…") and we were in fact lucky to get the data that we did. We are currently planning to repeat the experiment in Q2 of FY05.

The laboratory research activities described in this section were carried out under the auspices of an approved Integrated Work Sheet (IWS# 10537 r4, *Development of High Energy Neutron Radiography at Ohio University*, RI: J. Hall) and in accordance with all existing OUAL operational and radiation safety guidelines. Copies of these documents and/or additional information on personnel safety issues related to this work may be obtained directly from the authors of this report upon request.

CONCLUSIONS

The wide variety of unclassified neutron imaging experiments that we have done at OUAL over the past few years using our relatively simple prototype imaging detector, combined with a number of classified Monte Carlo simulations of potential CSA imaging scenarios, have demonstrated the potential effectiveness of high-energy neutron imaging and validated its proposed use as a nonintrusive inspection tool in ESC applications. The design of the RFQ/DTL accelerator system associated with the neutron source is complete and we are making good progress on the development of other key components including the high-pressure "windowless" D_2 gas target endstation and a full-scale prototype of the imaging detector. We are poised to commit to the construction of a full-scale neutron imaging system facility at LLNL when sufficient funds become available (note that procurement of the accelerator system will essentially drive the deployment schedule).

Several additional neutron imaging experiments (involving radiography *and* tomography) are planned at OUAL during the coming year as well as additional detailed Monte Carlo imaging simulations of classified systems and imaging scenarios. We expect to complete our current suite of tests involving the use of static gas in the prototype D_2 gas target endstation units by Q3 of FY05 and should be able to finalize the endstation design by the end of the FY. We also expect to issue a contract to a qualified vendor to fabricate a full-scale prototype of our proposed (large-format) neutron imaging detector during Q2 of FY05 and hope to be able to run acceptance tests on it at OUAL sometime before the end of the FY.

ACKNOWLEDGMENTS (U)

We would first like to thank Drs. William McLean and Bryan Balazs as members of the ESC management team at LLNL for their continued support and administrative guidance related to this project. We would also like to acknowledge Prof. David Ingram of Ohio University and the staff of OUAL for their support in facilitating neutron imaging experiments conducted there, Dr. Andrew Anderson and Kipp Whittaker of LLNL for their support in running ALE3D calculations relevant to the development of the D_2 gas target endstation and, finally, Kenneth Schwartz and Dr. William Moddeman of Pantex for supplying the IHE test object assembly used in the imaging experiment described here (not to mention the financial support that made the experiment possible in the first place...).

This work was performed at the University of California, Lawrence Livermore National Laboratory, under the auspices of the U.S. Department of Energy (contract # W-7405-Eng-48).

REFERENCES

1. F. Dietrich and J. Hall, "Detector concept for neutron tomography in the 10 - 15 MeV energy range", LLNL doc. UCRL-ID-123490 (LLNL, 1996).
2. F. Dietrich, J. Hall and C. Logan, "Conceptual design for a neutron imaging system for thick target analysis operating in the 10 - 15 MeV energy range," UCRL-JC-124401 (LLNL, 1996), published in *Proc. 14th Int. Conf. on the Application of Accelerators in Research and Industry* (Denton, TX, 1996), AIP **CP392**, ed. J. Duggan and I. Morgan, 837 (1997).
3. J. Hall, F. Dietrich, C. Logan and G Schmid, "Development of high-energy neutron imaging for use in NDE applications", UCRL-JC-134562 (LLNL, 1999), published in *Penetrating Radiation Systems and Applications* (Denver, CO, 1999), SPIE **3769**, ed. F. Doty, 31 (1999).
4. J. Hall, F. Dietrich, C. Logan and B. Rusnak, "Recent Results in the Development of Fast Neutron Imaging Techniques," UCRL-JC-140435 (LLNL, 2000), published in *Proc. 16th Int. Conf. on the Application of Accelerators in Research and Industry* (Denton, TX, 2000), AIP **CP576**, ed. J. Duggan and I. Morgan, 1113 (2001).
5. B. Rusnak and J. Hall, "An accelerator system for neutron radiography," UCRL-JC-139558 (LLNL, 2000), published in *Proc. 16th Int. Conf. on the Applications of Accelerators in Research and Industry* (Denton, TX, 2000), AIP **CP576**, ed. J. L. Duggan and I. L. Morgan, 1105 (2001).
6. J. Hall, "Uncovering hidden defects with neutrons," published in *Science & Technology Review*, May 2001 (LLNL, 2001).
7. R. Hamm, AccSys Technologies, Inc., private communication.
8. E. Iverson, R. Lanza and L. Lidsky, "Windowless gas targets for neutron production," *Proc. 5th Int. Conf. on Neutrons in Research and Industry* (Crete, Greece, 1996), SPIE **2867**, ed. G. Vourvopoulos, 513 (1996).
9. E. Iverson, "Windowless gas targets for neutron production," Ph.D. thesis (unpublished), Massachusetts Institute of Technology, Cambridge, MA, February 1997; R. Lanza, private communication.
10. W. Gerber, "Investigation of windowless gas target systems for particle accelerators," Master's thesis (unpublished), Massachusetts Institute of Technology, Cambridge, MA, June 1998; R. Lanza, private communication.
11. E. Empey, "Implementation of a closed-loop windowless gas target system for neutron production," Master's thesis (unpublished), Massachusetts Institute of Technology, Cambridge, MA, February 2000; R. Lanza, private communication.
12. J. Guzek, *et al.*, "Development of High-Pressure Deuterium Gas Targets for the Generation of Intense Monoenergetic Fast Neutron Beams," *Nuclear Instruments and Methods in Physics Research B*, **152**, 512 (1999).

COLLECTED FIGURES

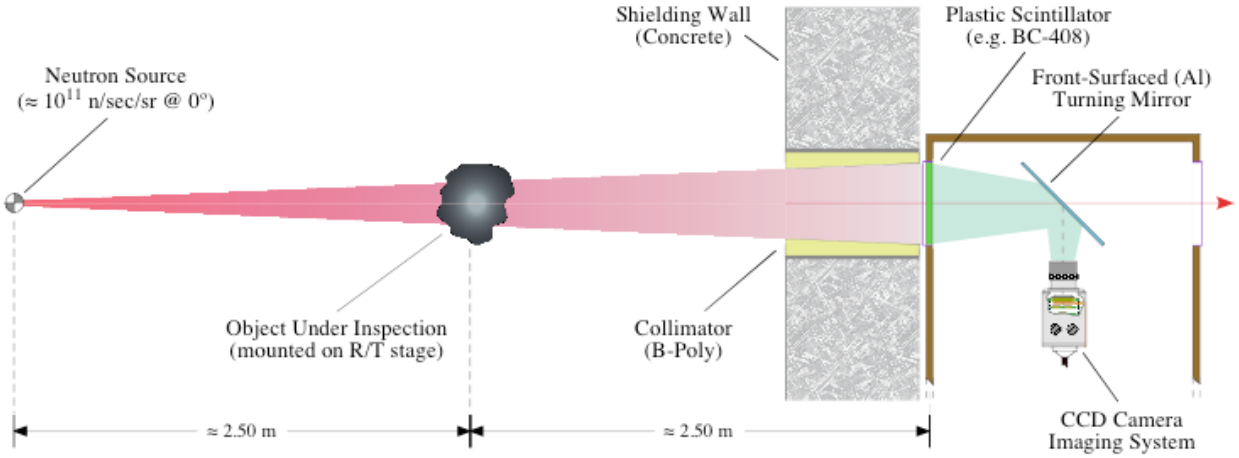

Figure 1: Conceptual design of proposed high-energy neutron imaging system. This particular representation shows the system with a 2:1 image magnification factor (which minimizes image noise caused by internal scattering within the object); however, a magnification factor of 1.25:1 (which offers improved spatial resolution) is also being considered. The objects will be mounted on a rotation/translation stage assembly that will allow either conventional radiographic or full CT imaging.

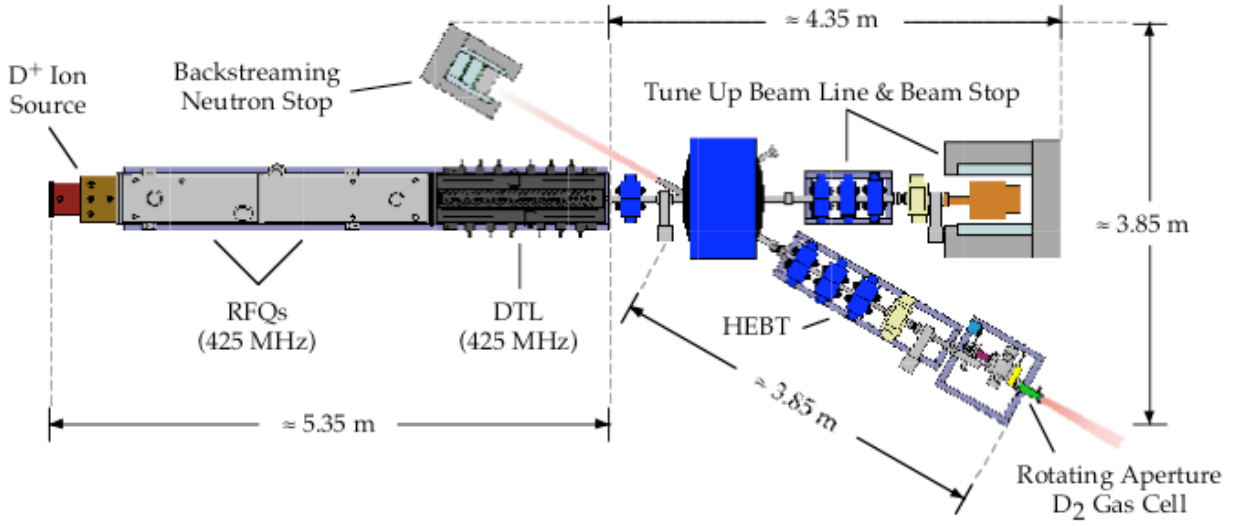

Figure 2: Schematic of proposed high-intensity neutron source. The full-scale, production-line system will consist of a D^+ ion source and a pair of compact, radio-frequency quadrupoles (RFQs) coupled to a short drift-tube linac (DTL). The high-energy beam transport (HEBT) system and D_2 gas target endstation are also shown along with a tune-up beam line and beam stop.

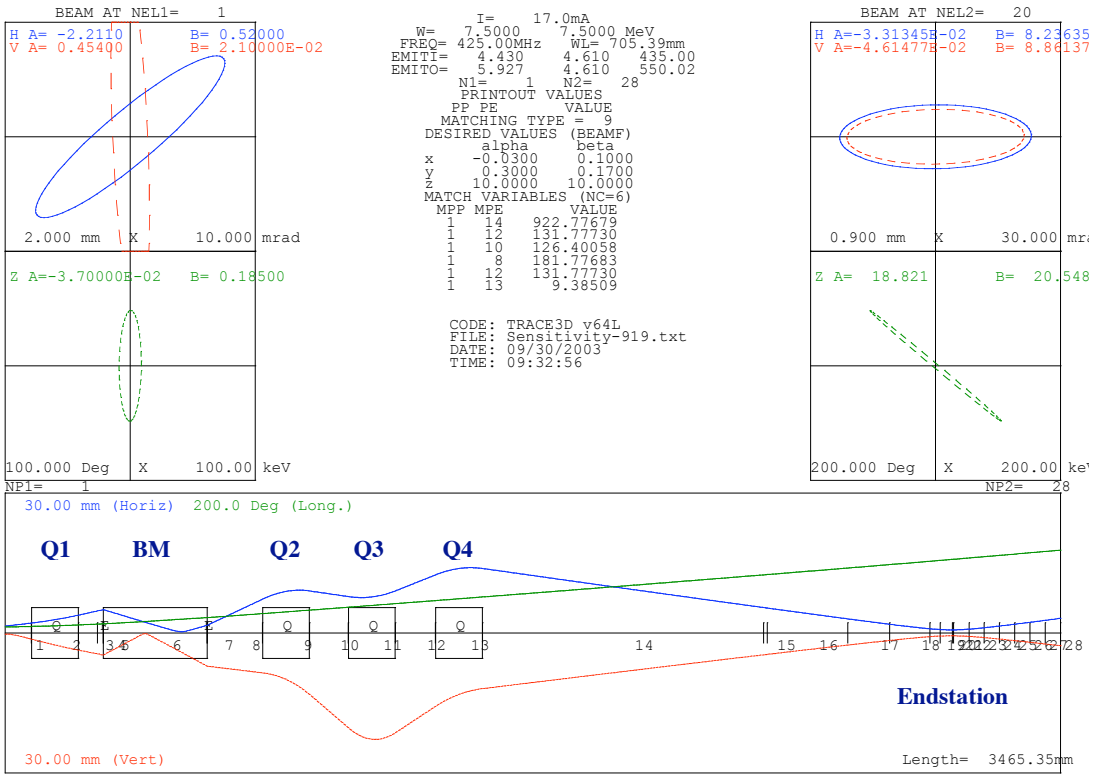

Figure 3: TRACE3D analysis of the conceptual HEBT design showing beam envelopes for ≈ 95% transmission through system. A horizontal plot is also shown which shows the relative positions of the first quadrupole, the bending magnet and the final quadrupole triplet designed to focus the beam into the target endstation (waist on the right).

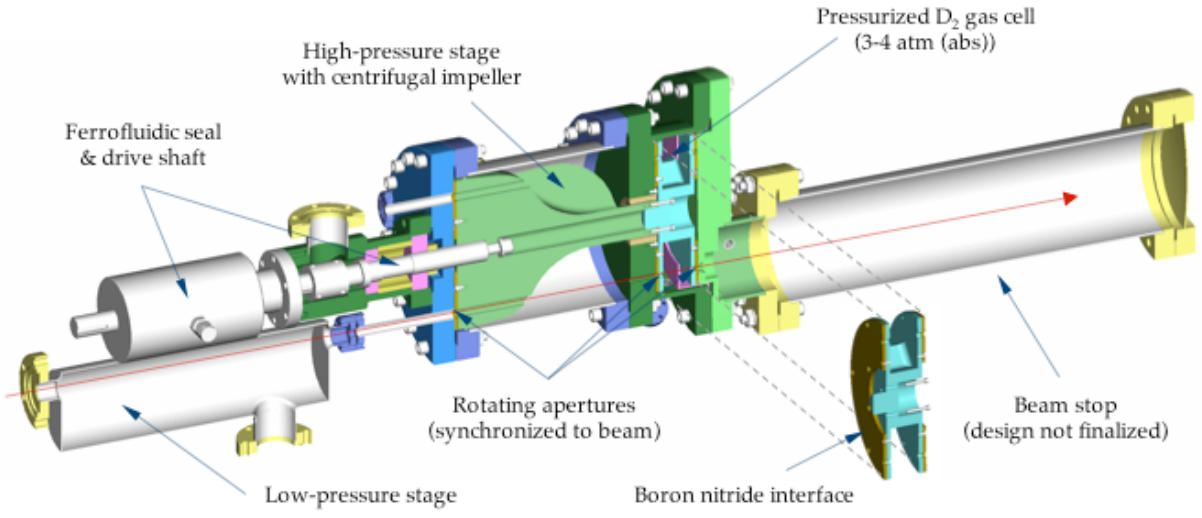

Figure 4: Initial design of "rotating-aperture" D_2 gas target endstation. The high-pressure sealing rotors were immersed in the D_2 target gas in this design to facilitate sealing and minimize pressure-induced pulsing of the rotors; however, the drive motor was located outside of the high-pressure stage which required the use of a Ferrofluidic seal on the vacuum feed-through.

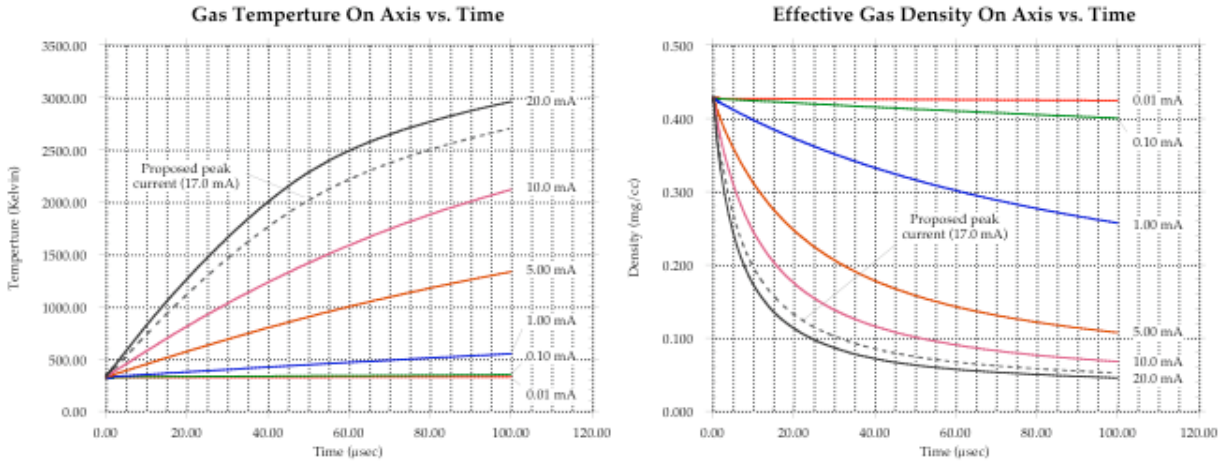

Figure 5: D_2 gas temperature and density vs. time in the beam focus channel for initial endstation design. These results indicated that, for peak beam currents in the 5 - 20 mA range, significant heating of the target gas would occur within 10's of μsec, causing a rapid drop in density along the beam channel ("burn through").

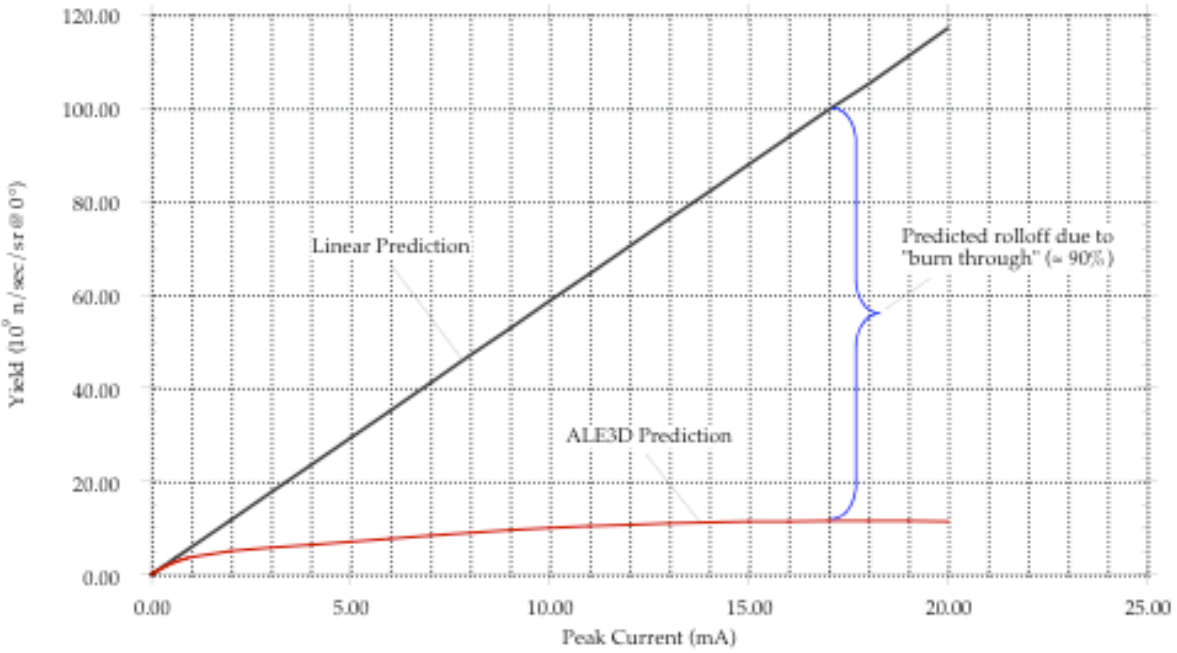

Figure 6: Predicted roll-off (relative to the expected value) in effective neutron yield due to D_2 density rarefactions associated with beam heating. Note that the roll-off for a peak current of ≈ 17 mA (*i.e.* our proposed system) could be ≈ 90% if no measures are taken to mitigate the rarefactions of the D_2 target gas.

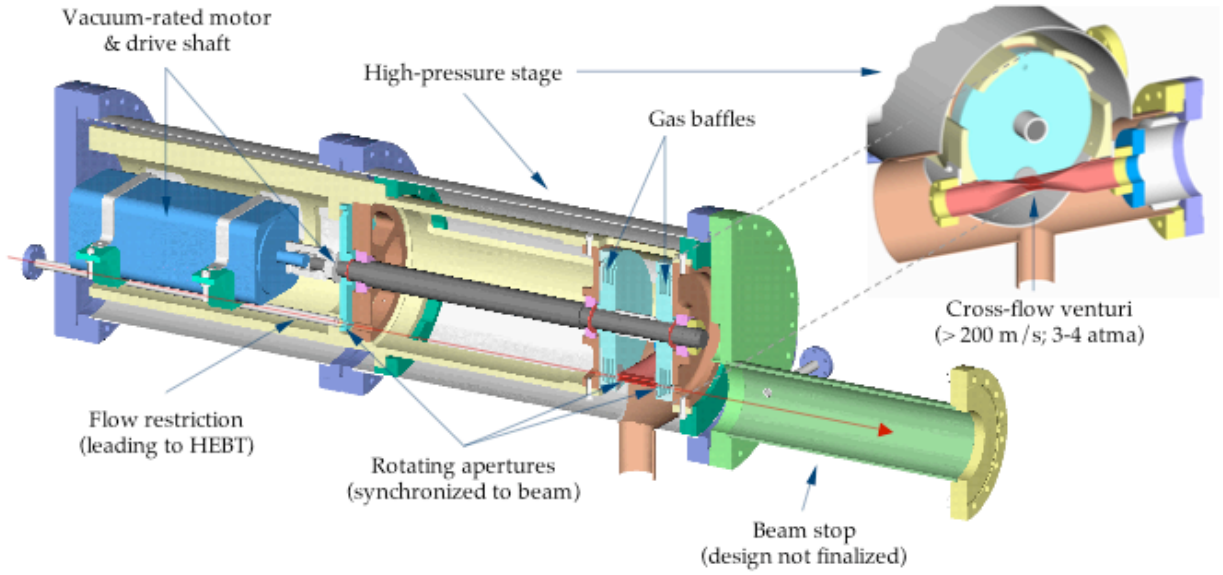

Figure 7: Revised design of "rotating-aperture" D_2 gas target endstation. A cross-flow D_2 venturi capped at either end by baffled, rotating apertures is used in this design to minimize the effect of density rarefactions associated with beam heating.

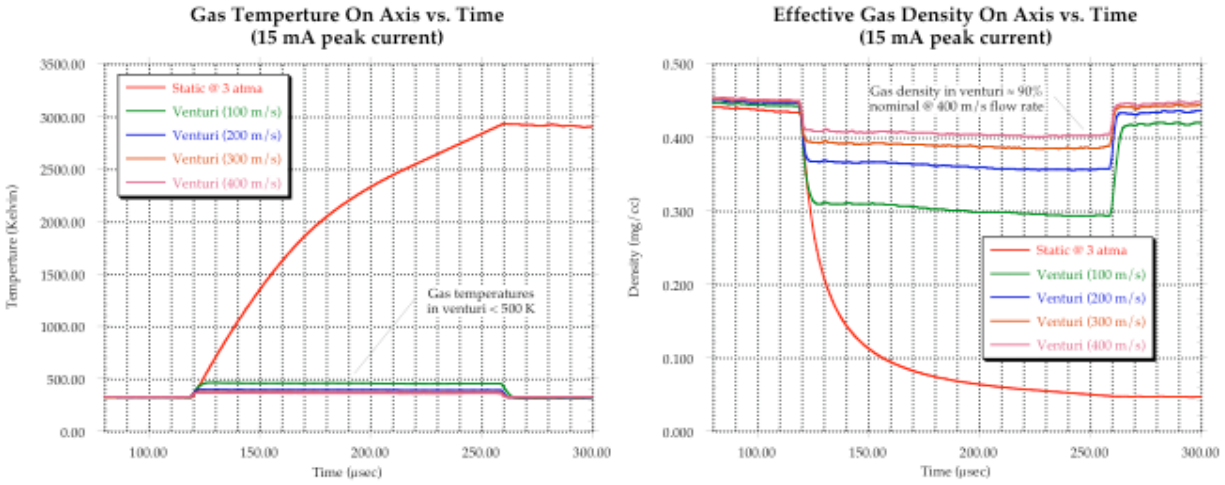

Figure 8: D_2 gas temperature and density vs. time in the beam focus channel for revised endstation design. These results indicated that it should be possible to maintain a D_2 gas density in the beam channel equivalent to an average pressure of ≈ 3 atma using reasonably-sized, commercially-available vacuum pumps and standard gas handling systems.

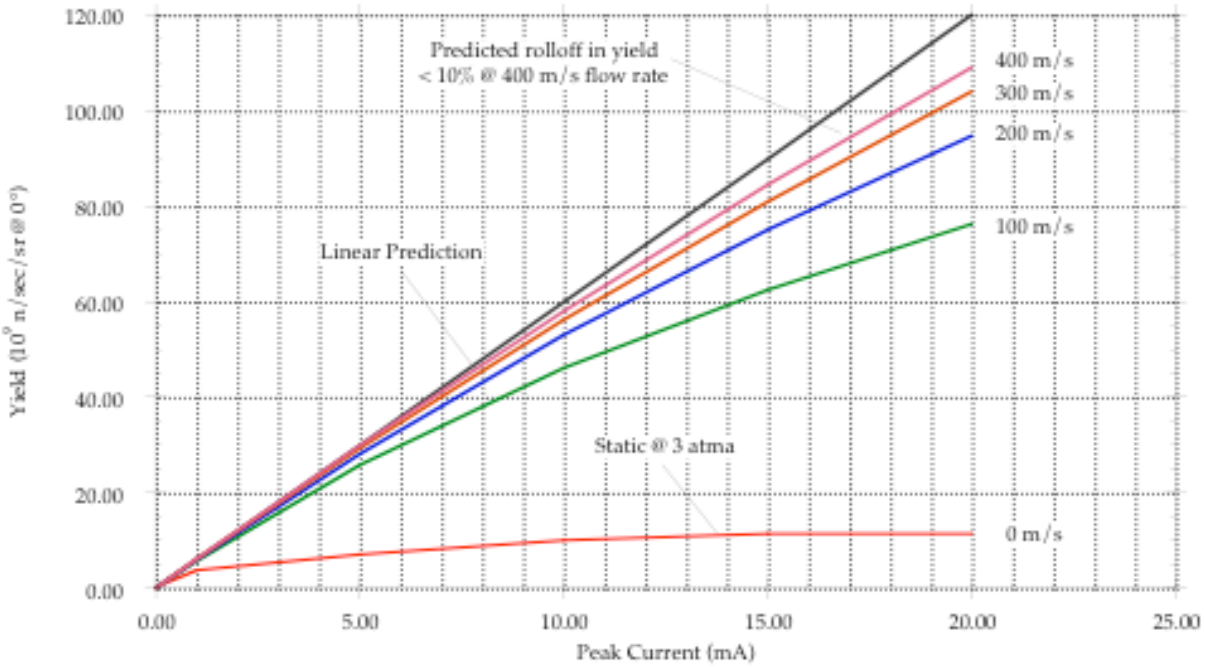

Figure 9: Predicted roll-off (relative to the expected value) in effective neutron yield due to D_2 density rarefactions associated with beam heating. Note that the roll-off for a peak current of ≈ 17 mA (*i.e.* our proposed system) is now predicted to be < 10% for a venturi gas flow rate of ≈ 400 m/s (achievable with our proposed system).

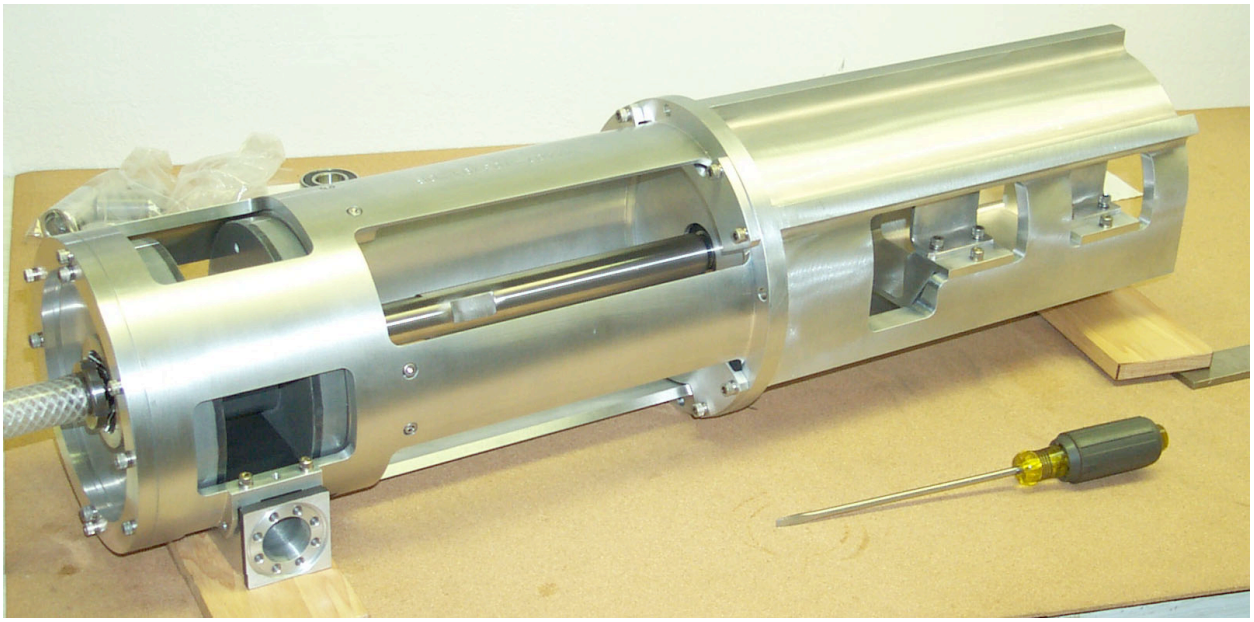

Figure 10: The first of two full-scale prototypes of the new target endstation fabricated by the CHAMP Company of Campbell, CA and delivered to LLNL for use in performance tests. The one-piece, rigid aluminum sub-frame shown here allows us to align and hold the drive motor and all of the various precision parts that need to rotate at ≈ 4000 RPM without the need to procure or fabricate special vacuum enclosures that can also be precision aligned.

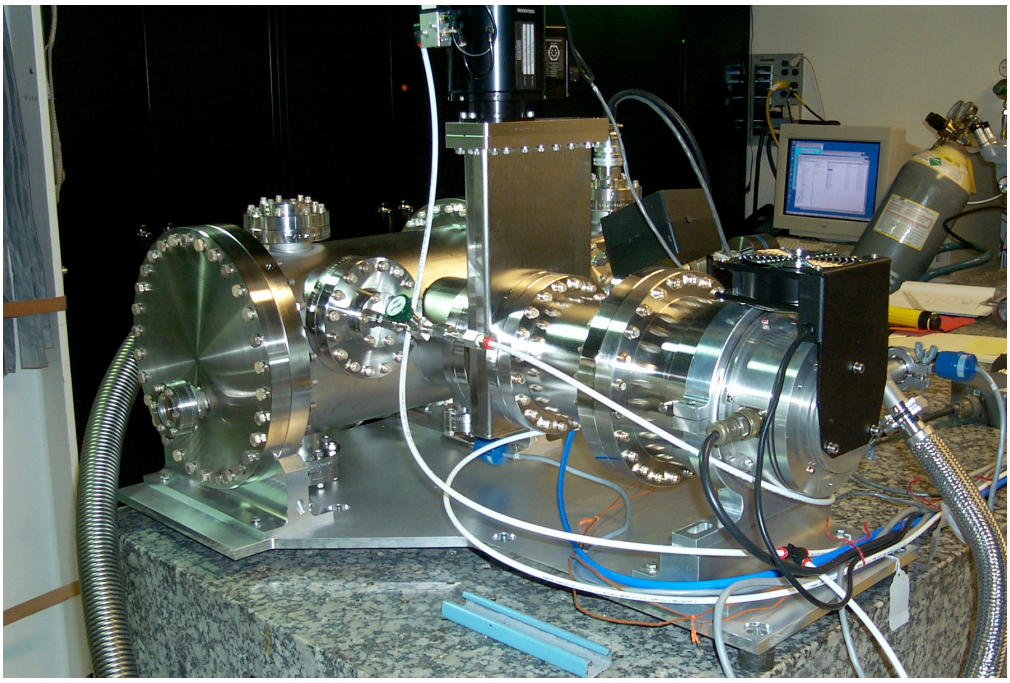

Figure 11: Rotating-aperture endstation assembly installed in vacuum enclosure equipped with pumps and diagnostic sensors.

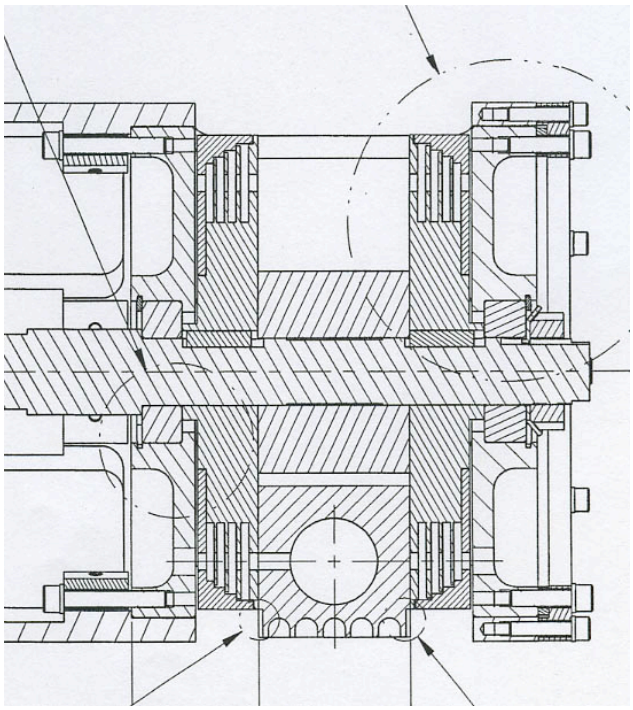

Figure 12: Design drawing of cross-flow region in endstation flanked by baffled rotors. One of the primary goals in designing and fabricating the test units was to verify that we could achieve a gap spacing of ≈ 0.001" between these components.

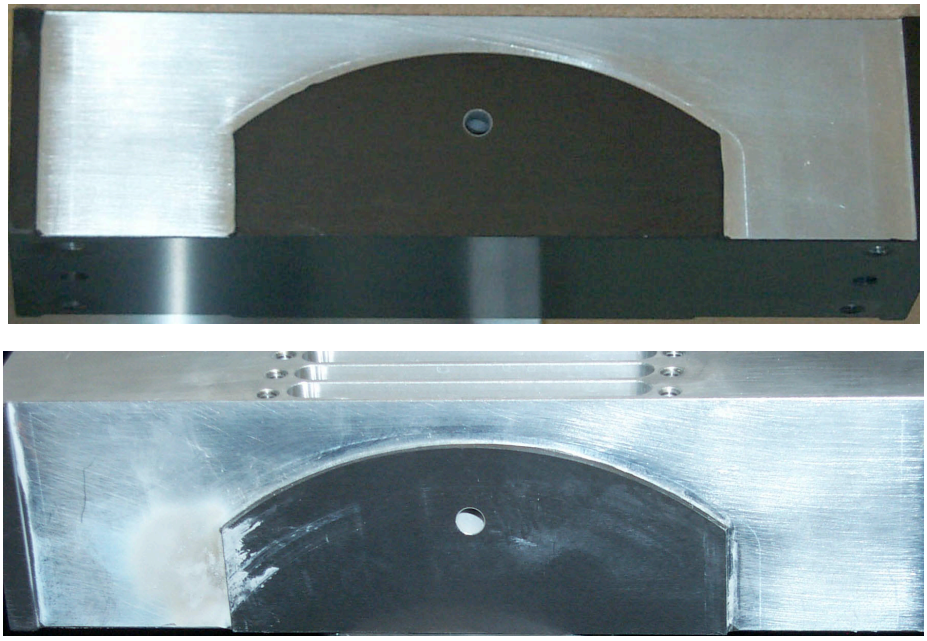

Figure 13: Pictures of precision-ground surface on cross-flow tube before (top) and after (bottom) running with high-pressure gas in the tube. A gradual build-up of powdered alumina between this surface and the opposing rotor slowly filled the narrow gap between the two pieces, eventually causing the system to seize up entirely and resulting in appreciable scoring on both surfaces. The source of the powder was discovered to be residual deposits of hardened alumina "mud" that had accumulated in the baffles of the rotors during the original surface grinding process and were then dislodged and pulverized by high-pressure shock waves passing through the apertures of the rotor during operation

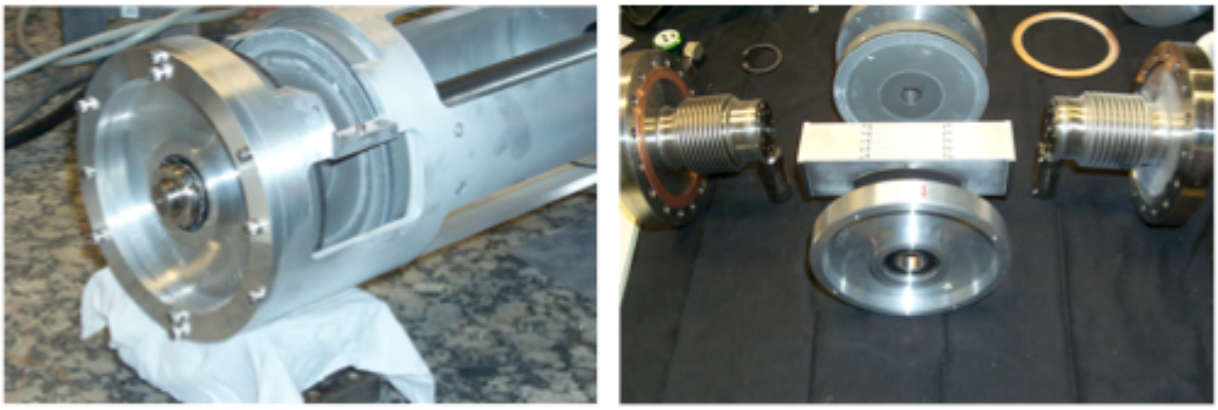

Figure 14: Pictures of endstation assembly before (top) and after (bottom) running with high-pressure gas in the tube. Note the build-up of dust on the aluminum sub-frame (cleaned prior to operation) and the powder on the right hand bellows assembly.

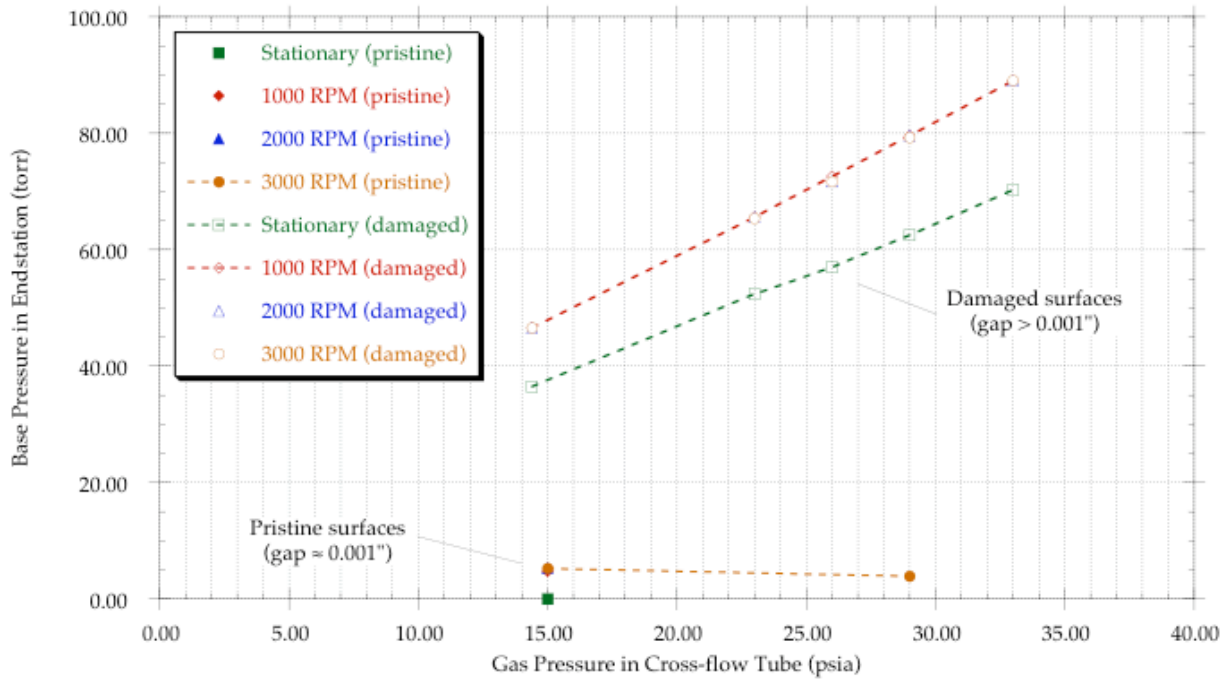

Figure 15: Initial pressure tests of rotating aperture system using static gas. Preliminary results obtained before the surfaces on the rotor and cross-flow tube were damaged indicate that we should be able to maintain a base pressure of < 10 - 20 torr in the high pressure pumping stage of the endstation using a few relatively inexpensive dry scroll pumps (our eventual goal is to reduce the base pressure in the endstation to ≤ 5 torr with ≈ 3 atma in the venturi of the gas cell). Note that increasing the rotor speed from 1000 RPM up to 3000 RPM seemed to have very little effect on the base pressure in the endstation.

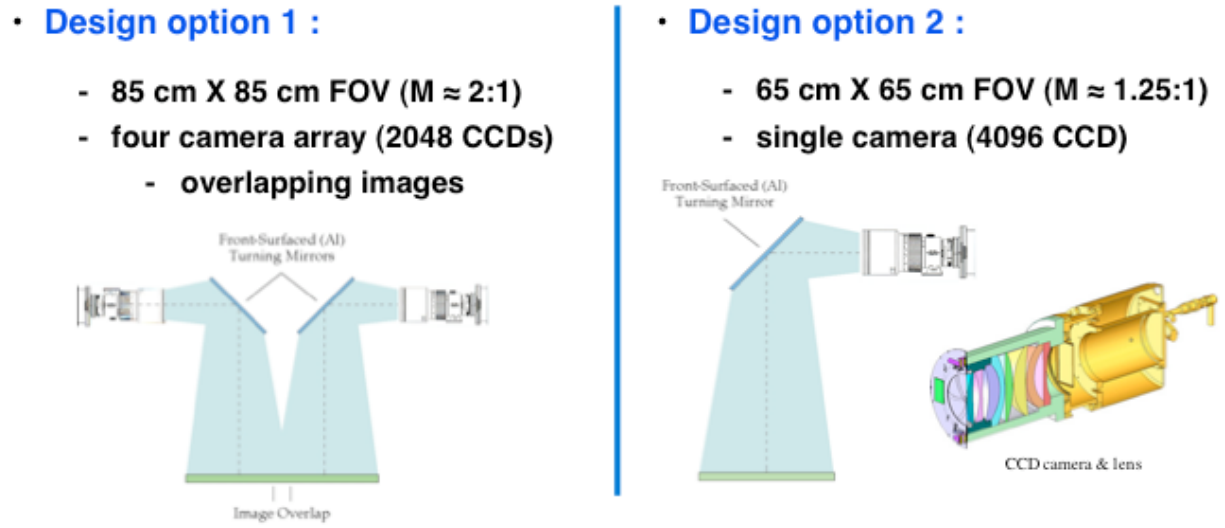

Figure 16: Design options for proposed full-scale imaging detector system. Option 1 (left) is similar to that currently being developed for use in ESC high-resolution x-ray imaging systems at Pantex. Image registration would be done using a dedicated control computer with final processing and analysis being done off-line in a secure environment. Option 2 (right) is a much simpler (and lower cost) design which offers comparable optical resolution but is limited to a somewhat smaller field of view. Final image processing and analysis would again be done off-line in a secure environment.

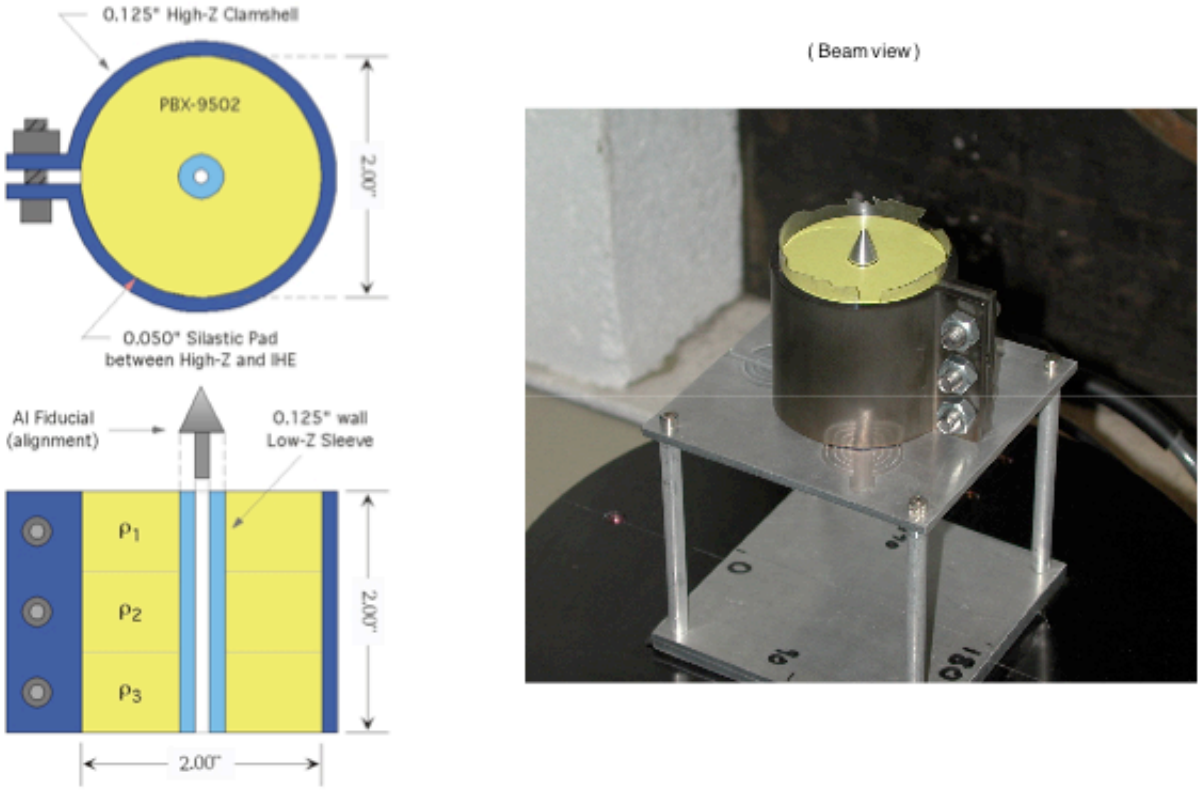

Figure 17: Segmented PBX-9502 IHE test object provided by Pantex for use in CT imaging experiments conducted at OUAL during FY04. The annular IHE cylinders (compressed to densities that differed by ≤ 0.06 g/cc overall) were stacked in groups of three and shielded by a high-Z (U6%Nb) clamshell on the outside and a low-Z (Be) sleeve on the inside.

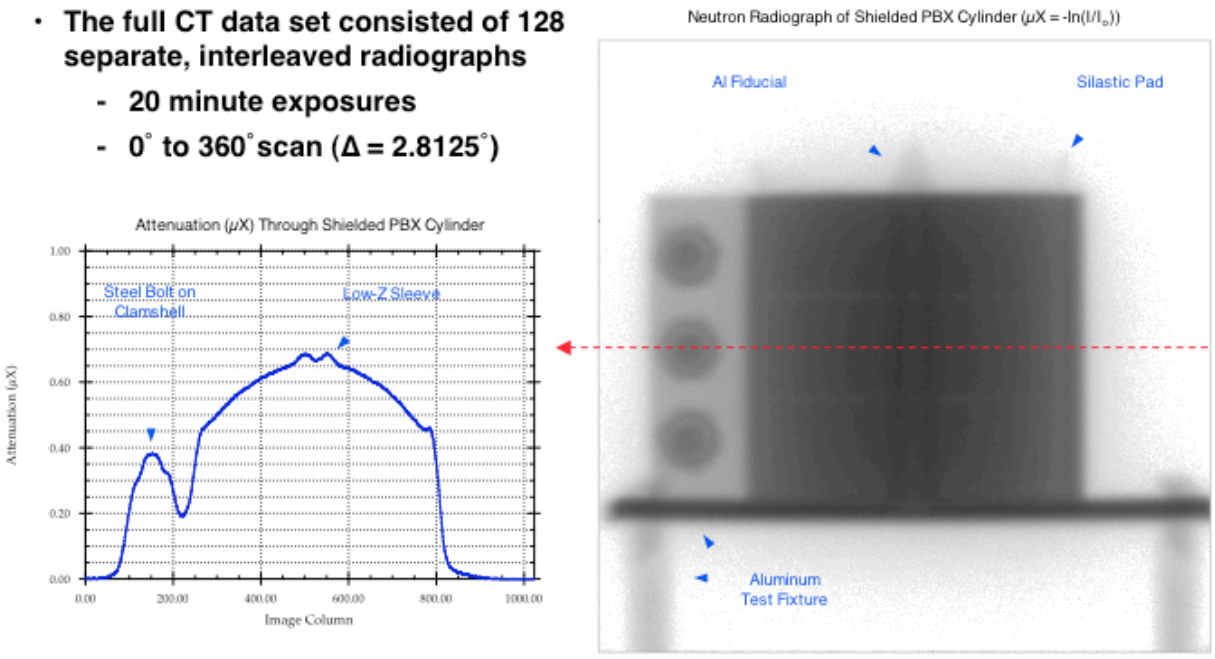

Figure 18: Typical neutron radiograph of test object. The CT imaging process (data acquisition and rotation stage control) was fully automated at OUAL using a custom LabView script running on the control computer.

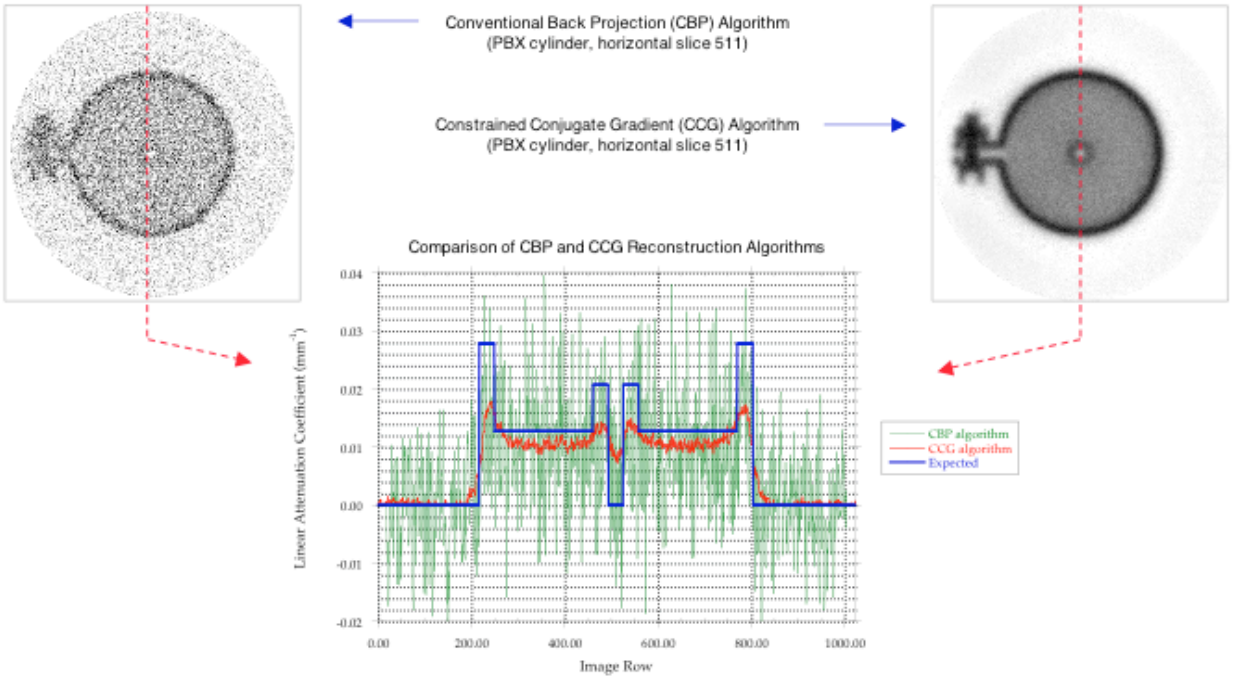

Figure 19: Comparison of Conventional Back Projection (CBP) and Constrained Conjugate Gradient (CCG) tomographic reconstruction algorithms. The CCG algorithm utilizes an iterative, constrained (*e.g.* $\mu X \geq 0$) least-squares fitting procedure which, while more CPU intensive than CBP, significantly reduces the overall statistical noise level in CT reconstructions.

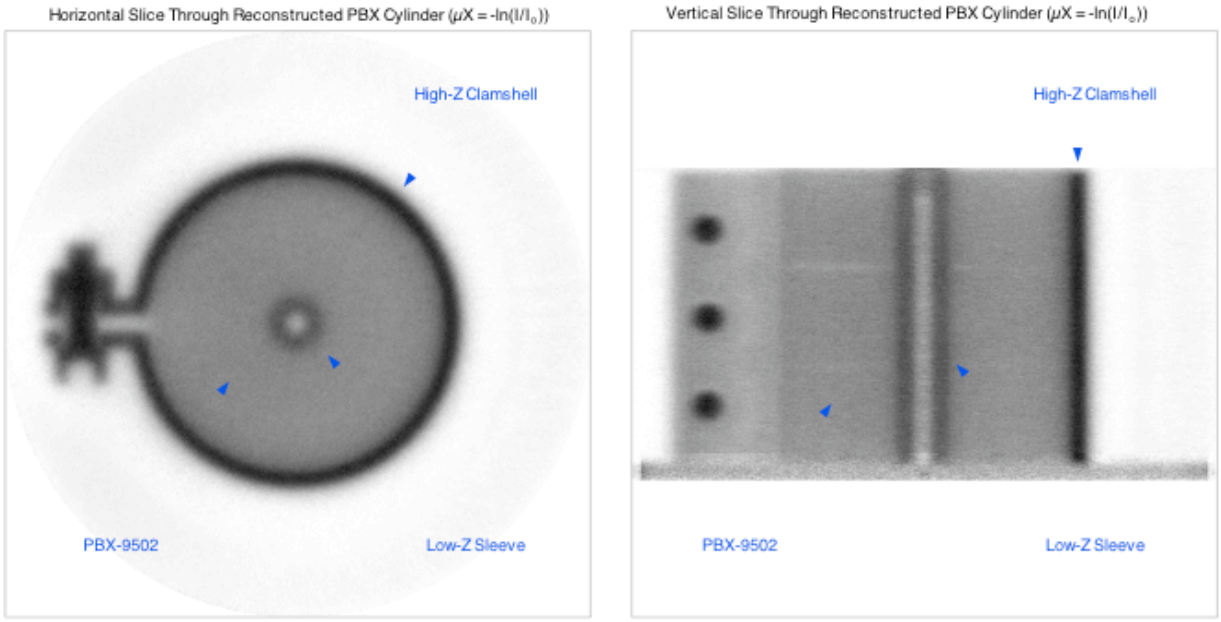

Figure 20: Tomographic reconstruction of test object done using LLNL's Constrained Conjugate Gradient (CCG) algorithm. The primary structural features in the object - including even the bond joints between the three shielded IHE segments - are clearly visible in slices taken through the reconstructed object.